ARTICLE

doi:10.1038/nature15514

Cleavage of GSDMD by inflammatory caspases determines pyroptotic cell death

Jianjin Shi[1,2]*, Yue Zhao[2]*, Kun Wang[2], Xuyan Shi[2], Yue Wang[2], Huanwei Huang[2], Yinghua Zhuang[2], Tao Cai[2], Fengchao Wang[2] & Feng Shao[2,3,4]

Inflammatory caspases (caspase-1, -4, -5 and -11) are critical for innate defences. Caspase-1 is activated by ligands of various canonical inflammasomes, and caspase-4, -5 and -11 directly recognize bacterial lipopolysaccharide, both of which trigger pyroptosis. Despite the crucial role in immunity and endotoxic shock, the mechanism for pyroptosis induction by inflammatory caspases is unknown. Here we identify gasdermin D (*Gsdmd*) by genome-wide clustered regularly interspaced palindromic repeat (CRISPR)-Cas9 nuclease screens of caspase-11- and caspase-1-mediated pyroptosis in mouse bone marrow macrophages. GSDMD-deficient cells resisted the induction of pyroptosis by cytosolic lipopolysaccharide and known canonical inflammasome ligands. Interleukin-1β release was also diminished in *Gsdmd*$^{-/-}$ cells, despite intact processing by caspase-1. Caspase-1 and caspase-4/5/11 specifically cleaved the linker between the amino-terminal gasdermin-N and carboxy-terminal gasdermin-C domains in GSDMD, which was required and sufficient for pyroptosis. The cleavage released the intramolecular inhibition on the gasdermin-N domain that showed intrinsic pyroptosis-inducing activity. Other gasdermin family members were not cleaved by inflammatory caspases but shared the autoinhibition; gain-of-function mutations in *Gsdma3* that cause alopecia and skin defects disrupted the autoinhibition, allowing its gasdermin-N domain to trigger pyroptosis. These findings offer insight into inflammasome-mediated immunity/diseases and also change our understanding of pyroptosis and programmed necrosis.

Inflammatory caspases (caspase-1, murine caspase-11 and human caspase-4/5) are crucial for innate immune defences. Aberrant or excessive activation of caspase-1 causes or is associated with many autoinflammatory, autoimmune and even metabolic diseases[1,2]. Caspase-1 is activated by the canonical inflammasomes, in which a central scaffold, such as NLRP3, NLRP1, NAIP–NLRC4, AIM2 and Pyrin, detects its cognate ligand[1]. The NAIPs directly recognize flagellin, as well as the rod and needle components of bacterial type III secretion system (T3SS)[3–5]. The newly identified Pyrin inflammasome indirectly senses bacterial modifications and inactivation of host Rho GTPases[6]. Caspase-11 detects cytosolic bacterial lipopolysaccharide (LPS), playing a critical role in endotoxic shock[7,8]. Caspase-11 and its human counterparts caspase-4/5 are activated by direct LPS binding[9,10].

Caspase-1 activation mainly occurs in macrophage/dendritic cells. Active caspase-1 processes and maturates interleukin (IL)-1β/18 and also triggers a form of programmed necrosis known as pyroptosis. Pyroptosis is the dominant response upon caspase-4/5/11 activation, occurring in both macrophage and non-macrophage cells[9,11]. Pyroptosis features pore formation in the plasma membrane, cell swelling and rupture of the membrane, causing massive leakage of cytosolic contents. Accumulating evidences suggest a critical role of pyroptosis in immunity and disease[12]. Pyroptosis of infected cells releases intracellular bacteria for neutrophil-mediated killing[13]. Inflammasome-mediated, but IL-1β/18-independent, clearance of infection has been noted with several intracellular bacteria[12–15]. Pyroptosis induced by the NLRP1B inflammasome or a gain-of-function mutation in *Nlrp1a* is the primary cause of anthrax-lethal-toxin-induced lung injury[16] and haematopoietic progenitor cell depletion in mice[17], respectively. Caspase-1-mediated pyroptosis in HIV infection accounts for $CD4^+$ T-cell depletion[18], a critical event in HIV pathogenesis. Pyroptosis rather than cytokine secretion is probably the key determinant of mouse lethality caused by systemic activation of the NAIP–NLRC4 inflammasome or caspase-11 activation by excessive LPS[7,8,19]. Despite these important functions, the mechanism underlying how inflammatory caspases trigger pyroptosis is unknown.

GSDMD is required for LPS-induced pyroptosis

We previously established an LPS electroporation protocol that can induce pyroptosis in more than 90% of LPS-stimulated cells[9]. This robust assay allowed for unbiased genome-wide genetic screen using the CRISPR-Cas9 technology to identify new components in LPS/caspase-4/11-induced pyroptosis. The screen was performed in *Tlr4*$^{-/-}$ immortalized bone-marrow-derived macrophages (iBMDMs) that responded normally to LPS electroporation (Extended Data Fig. 1a). As expected, three out of the four *Casp11*-targeting guide RNAs (gRNAs) were recovered within the top 100 hits. Notably, there was only one other gene gasdermin D (*Gsdmd*) that also had multiple gRNA hits; four out of the five *Gsdmd*-targeting gRNAs appeared in the top 30 hits, with two among the top 10 (Fig. 1a). GSDMD is conserved in human and mouse with ~72% sequence similarity (Extended Data Fig. 2a). Small interference RNA (siRNA) knockdown in HeLa cells excluded other selected top hits but confirmed the requirement of *GSDMD* (Extended Data Fig. 1b–d, also see Methods). siRNA knockdown of *Gsdmd* in mouse iBMDMs also inhibited LPS-induced pyroptosis; the extent of inhibition by three different siRNAs correlated with their knockdown efficiency (Extended Data Fig. 1e, f).

[1]Peking University-Tsinghua University-National Institute of Biological Sciences Joint Graduate Program, School of Life Sciences, Tsinghua University, 100084, China. [2]National Institute of Biological Sciences, Beijing 102206, China. [3]National Laboratory of Biomacromolecules, Institute of Biophysics, Chinese Academy of Sciences, Beijing 100101, China. [4]National Institute of Biological Sciences, Beijing, Collaborative Innovation Center for Cancer Medicine, Beijing 102206, China.
*These authors contributed equally to this work.

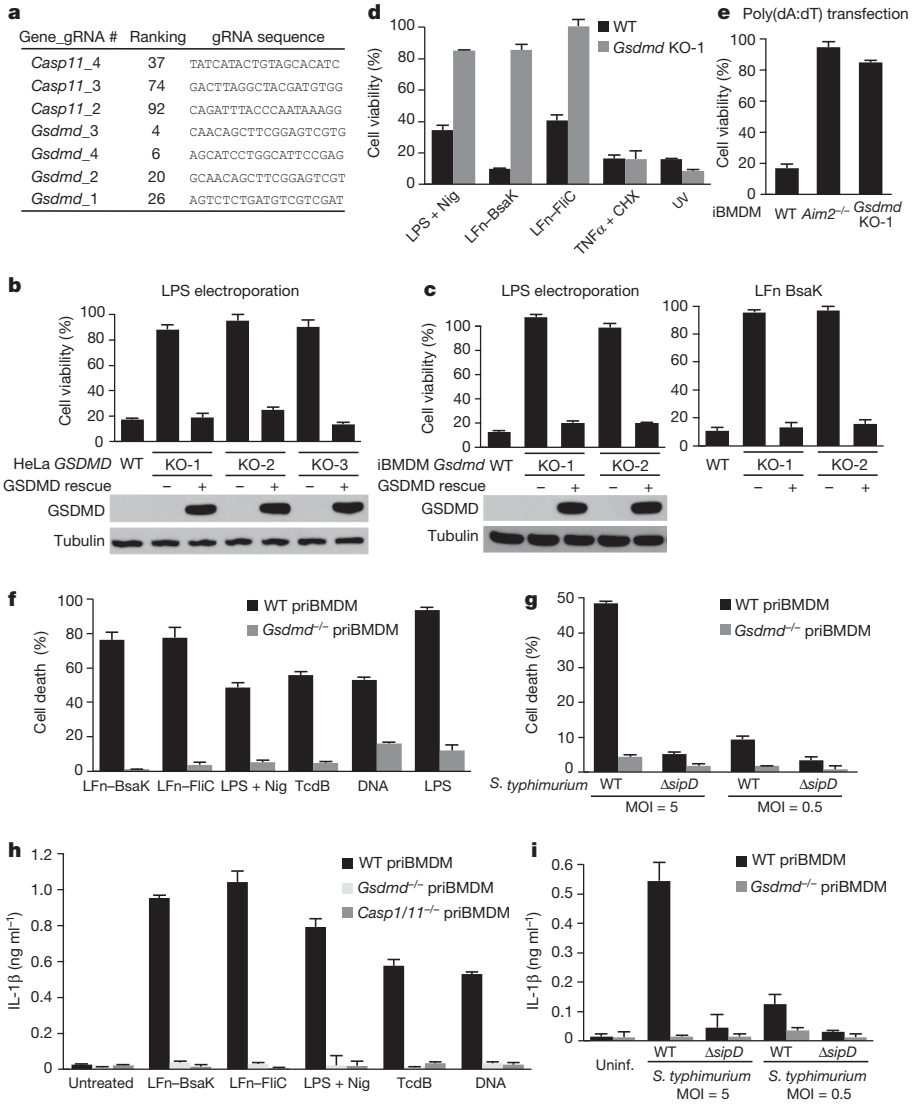

Figure 1 | Genetic screens identify that GSDMD is required for inflammatory-caspase-mediated pyroptosis and its role in caspase-1-induced IL-1β release. **a**, gRNA hits from a genome-wide CRISPR-Cas9 screen of LPS-induced pyroptosis in mouse iBMDMs. Shown are genes with multiple gRNA hits among the top 100 hits. Fold-enrichment-based ranking and the target sequence of each gRNA are listed. **b**, **c**, Effects of *GSDMD* knockout on LPS electroporation and LFn–BsaK-induced pyroptosis. Three *GSDMD*$^{-/-}$ HeLa clones (KO-1, -2 and -3) and two *Gsdmd*$^{-/-}$ iBMDM clones generated by CRISPR-Cas9-mediated targeting were analysed. For complementation, Flag-tagged human GSDMD was stably expressed in the knockout cells and its expression is shown by anti-Flag immunoblotting; tubulin expression is the loading control. WT, wild type. **d**, **e**, Effects of *Gsdmd* knockout on canonical inflammasome-mediated pyroptosis or on apoptosis. LFn–BsaK, LFn–FliC (flagellin), LPS + Nig. (nigericin), poly(dA:dT) transfection, TNFα + CHX and ultraviolet (UV) radiation were employed to activate the NAIP2–NLRC4, the NAIP5–NLRC4, the NLRP3, the AIM2 inflammasome, the extrinsic and the intrinsic apoptosis pathways, respectively. **f**–**i**, Assays for inflammasome-mediated pyroptosis and IL-1β release. Primary BMDMs (priBMDMs) from wild-type or *Gsdmd*$^{-/-}$ mice were stimulated with indicated canonical inflammasome stimuli or LPS electroporation (**f**, **h**), or infected with *S. typhimurium* (wild-type or the T3SS-deficient Δ*sipD* mutant) at the indicated multiplicity of infection (MOI) (**g**, **i**).TcdB, *C. difficile* toxin B; Uninf., uninfected cells. ATP-based cell viability (**b**–**e**), lactate dehydrogenase (LDH)-release-based cell death (**f**, **g**), and ELISA assay of IL-1β release (**h**, **i**) are expressed as mean values ± s.d. from three technical replicates. Data shown are representative of at least three (**b**–**e**) or two (**f**–**i**) independent experiments.

To further validate the role of GSDMD, *GSDMD*$^{-/-}$ HeLa cells and *Gsdmd*$^{-/-}$ iBMDM cells were generated by CRISPR-Cas9-mediated targeting (Extended Data Fig. 3a). In both cells, the absence of GSDMD completely blocked LPS electroporation-triggered pyroptosis, which was confirmed in multiple knockout clones (Extended Data Fig. 3b, c). Re-expression of human GSDMD in three *GSDMD*$^{-/-}$ HeLa cell clones all restored LPS-induced pyroptosis (Fig. 1b). Mouse GSDMD showed the same rescue effect (Extended Data Fig. 3d). Similarly, *Gsdmd*$^{-/-}$ iBMDM cells regained the sensitivity to LPS electroporation when complemented with either human or mouse GSDMD (Fig. 1c and Extended Data Fig. 3e).

GSDMD is required for caspase-1-mediated pyroptosis

We also performed a parallel CRISPR-Cas9 screen on caspase-1-mediated pyroptosis in iBMDM cells using the anthrax lethal factor N-terminal-domain-fused T3SS rod protein of *Burkholderia thailandensis* (LFn–BsaK), the most potent agonist of the NAIP–NLRC4 inflammasome[4,20]. Notably, the top hits recovered from the screen were dominated by gRNAs targeting all known components in the pathway, including *Naip2*, *Nlrc4* and *Casp1*, each of which was hit by multiple gRNAs (Extended Data Fig. 4a). The screen also hit *Gsdmd* which, along with seven other genes, had two independent gRNAs (Extended Data Fig. 4a). The requirement of *Gsdmd*, but not the seven other genes, for LFn–BsaK-induced pyroptosis was confirmed by siRNA knockdown assays (Extended Data Fig. 1e, f and 4b). Furthermore, *Gsdmd*$^{-/-}$ iBMDM clones completely resisted LFn–BsaK-induced pyroptosis (Extended Data Fig. 3f), which was fully restored by exogenous expression of GSDMD (Fig. 1c). *Gsdmd*$^{-/-}$ iBMDMs were also unresponsive to stimulation by LFn–flagellin (FliC), an agonist of the NAIP5–NLRC4 inflammasome (Fig. 1d). Caspase-7 was previously shown to be cleaved by caspase-1 upon inflammasome activation by flagellin in *Legionella pneumophila*-infected mouse macrophages[21]. We confirmed the cleavage of caspase-7/3 in LFn–BsaK-stimulated *Gsdmd*$^{-/-}$ iBMDMs (Extended Data Fig. 4c). However, evident cleavage could be observed 6 h after stimulation, a time point when *Gsdmd*-proficient cells had already died of pyroptosis (therefore little caspase-3/7 cleavage occurred). This suggests that caspase-3/7 cleavage plays no role in caspase-1-mediated pyroptosis, but may induce apoptosis or have other functions in defence against *L. pneumophila*[21]. Thus, GSDMD plays a critical role in caspase-1-mediated pyroptosis downstream of the NAIP–NLRC4 inflammasome.

GSDMD is only required for pyroptotic cell death

We further examined the role of GSDMD in other canonical-inflammasome-triggered pyroptosis. *Gsdmd*$^{-/-}$ completely blocked iBMDM cell pyroptosis upon activation of the NLRP3 and AIM2 inflammasomes by LPS plus nigericin and poly(dA:dT), respectively (Fig. 1d, e). In contrast, *Gsdmd*$^{-/-}$ did not affect extrinsic and intrinsic apoptosis triggered by TNFα plus cycloheximide (TNFα + CHX) and

ultraviolet irradiation, respectively (Fig. 1d). siRNA knockdown of *GSDMD* in HT-29 cells, though efficiently blocking LPS-induced pyroptosis, had no effect on TSZ (TNFα plus SMAC mimetic and the caspase inhibitor zVAD)-induced necroptosis, another form of programmed necrosis mediated by the RIPK1–RIPK3–MLKL axis[22] (Extended Data Fig. 5a–c).

We generated GSDMD-deficient mice by CRISPR-Cas9-mediated targeting. Primary BMDMs from two independent homozygous mutant mice (F1-1 and F1-2) (Extended Data Fig. 6a) were analysed for inflammasome activation, and similar results were obtained. In the canonical inflammasome pathway, pyroptosis mediated by the NAIP2/5–NLRC4, NLRP3 and AIM2 inflammasomes were all blocked by GSDMD deficiency (Fig. 1f). *Gsdmd*$^{-/-}$ also abolished pyroptosis upon *Clostridium difficile* toxin B activation of the Pyrin inflammasome[6]. Similarly, *Gsdmd*$^{-/-}$ BMDMs resisted LPS-induced pyroptosis (Fig. 1f). When infected with *Salmonella typhimurium*, wild-type BMDMs showed extensive pyroptosis due to T3SS-dependent activation of NAIP–NLRC4 inflammasome, but little pyroptosis occurred in BMDMs from *Gsdmd*$^{-/-}$ mice (Fig. 1g). Defective pyroptosis in *Gsdmd*$^{-/-}$ BMDMs was not due to the absence of caspase-1/11 expression (Extended Data Fig. 6b). Consistent with that in iBMDMs, primary *Gsdmd*$^{-/-}$ BMDMs remained sensitive to necroptosis induction by TSZ or LPS plus zVAD (Extended Data Fig. 5d, e). These data highlight a specific role of GSDMD in caspase-4/11 and caspase-1-mediated pyroptosis downstream of multiple inflammasomes.

GSDMD controls IL-1β release but not maturation

IL-1β maturation and secretion is the other major response of canonical inflammasome activation. We observed that primary *Gsdmd*$^{-/-}$ BMDMs, in contrast to wild-type BMDMs, secreted little IL-1β into the supernatant upon activation of the NAIP2/5–NLRC4, NLRP3, Pyrin and AIM2 inflammasomes (Fig. 1h). *S. typhimurium*-infection-induced IL-1β release was also inhibited in *Gsdmd*$^{-/-}$ BMDMs (Fig. 1i). Notably, caspase-1 autoprocessing occurred normally in *Gsdmd*$^{-/-}$ BMDMs upon activation of the above inflammasomes while extracellular secretion of both pro-caspase-1 and the mature caspase-1 was severely inhibited (Extended Data Fig. 6c). Intact caspase-1 autoprocessing and IL-1β maturation were also observed in the cytosol of *Gsdmd*$^{-/-}$ iBMDMs upon canonical inflammasomes activation (Fig. 2a, b and Extended Data Fig. 7a). Thus, GSDMD-mediated pyroptosis plays an important role in mature IL-1β release without affecting its maturation.

GSDMD is specifically cleaved by caspase-1/4/5/11

The above analyses predict that GSDMD functions downstream of the inflammatory caspases. We observed that GSDMD was cleaved in LPS and LFn–BsaK-stimulated HeLa and iBMDM cells, respectively (Fig. 2c). A cleavage product (~38 kDa) corresponding to the N-terminal half of 2×Flag–HA–GSDMD was constantly identified. LPS and LFn–BsaK-induced GSDMD cleavage was diminished by a pan-caspase inhibitor zVAD that also blocked cell death (Extended Data Fig. 7b). Co-expression of GSDMD with caspase-1, 4, 5 or 11 but not apoptotic caspases (caspase-2, 8 and 9) in 293T cells induced the same cleavage of GSDMD (Extended Data Fig. 7c). No GSDMD cleavage occurred in TNFα + CHX and TSZ-stimulated cells (Extended Data Fig. 5f), consistent with that GSDMD was not required for apoptosis and necroptosis (Fig. 1d and Extended Data Fig. 5c).

We then tested whether GSDMD is a direct substrate of inflammatory caspases. The active tetramer forms of caspase-1, 4 and 11, but not caspase-2, 8 and 9, were found capable of cleaving purified recombinant GSDMD (no tag, ~53 kDa) (Fig. 2d). The larger-size cleavage product migrated at ~31 kDa, which plus the 7-kDa 2×Flag–HA tag equals the 38-kDa N-terminal cleavage product observed in cells (Fig. 2c). The other cleavage product (~22 kDa) matched the size of the remaining C-terminal fragment. Consistent with that caspase-4/11

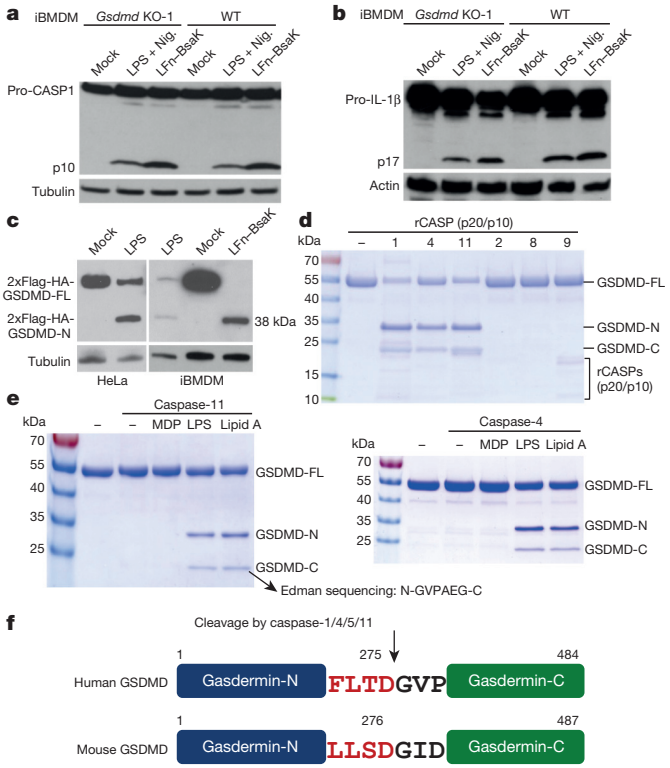

Figure 2 | GSDMD is a substrate specifically for inflammatory caspases. **a**, **b**, Effects of *Gsdmd* knockout on intracellular processing of caspase-1 and IL-1β (stably expressed).p10, mature caspase-1; Pro-CASP1, caspase-1 precursor; Pro-IL-1β, IL-1β precursor; p17, mature IL-1β. **c**, A specific cleavage in GSDMD induced by LPS electroporation and LFn–BsaK. GSDMD-FL, full-length GSDMD. **d**, *In vitro* cleavage of GSDMD by recombinant caspases. Purified GSDMD was incubated with active p20/p10 tetramers of indicated caspases (rCASPs). **e**, *In vitro* cleavage of GSDMD by LPS-activated caspase-11/4. Purified GSDMD was incubated with insect-cell-purified caspase-11/4 pre-incubated with LPS or indicated ligands. The N-terminal sequence of GSDMD-C determined by Edman sequencing is shown. **f**, Cartoon diagram of GSDMD structure and the cleavage by inflammatory caspases. LFn–BsaK and LPS + Nig. were used to activate the NAIP2–NLRC4 and NLRP3 inflammasome, respectively (**a**–**c**). 2×Flag-HA-GSDMD was stably expressed in HeLa and iBMDM cells (**c**). Reaction samples were analysed by SDS–PAGE and Coomassie blue staining (**d**, **e**). Cell lysates were subjected to anti-caspase-1 (**a**), anti-IL-1β (**b**), anti-Flag (**c**), anti-tubulin (**a**, **c**) and anti-actin (**b**) immunoblotting. All data shown are representative of three independent experiments.

are activated by direct LPS binding[9], insect-cell-purified caspase-11 could process recombinant GSDMD into the 31 kDa and 22 kDa fragments only upon prior incubation with LPS or Lipid A but not muramyl dipeptide (MDP) (Fig. 2e). Identical results were observed with insect-cell-purified caspase-4. Edman sequencing of the C-terminal fragment revealed an N-terminal sequence of $_{276}$GVPAEG$_{281}$ (Fig. 2e). Preceding $_{276}$GVPAEG$_{281}$ is $_{272}$FLTD$_{275}$ in human GSDMD and $_{273}$LLSD$_{276}$ in mouse GSDMD (Fig. 2f), which fit well with the substrate recognition motif of inflammatory caspases[23]. $_{272}$FLTD$_{275}$ is the only possible inflammatory-caspase cleavage site conserved in human and mouse GSDMD (Extended Data Fig. 2a). Thus, inflammatory caspases specifically cleave GSDMD after the $_{272}$FLTD$_{275}$ (or $_{273}$LLSD$_{276}$) sequence (Fig. 2f).

Cleavage of GSDMD is required for pyroptosis

We generated a mutant GSDMD, in which Asp275 (Asp276 in mouse GSDMD) was replaced with an alanine. As expected, the D/A mutants of GSDMD resisted cleavage by caspase-1 and caspase-4/5/11 overexpressed in 293T cells (Extended Data Fig. 8a, b). Physiologically

activated caspase-1 by LFn–BsaK also failed to cleave GSDMD D275A complemented into the *Gsdmd*$^{-/-}$ iBMDMs (Fig. 3a); importantly, the mutant was completely inactive in restoring LFn–BsaK-induced pyroptosis (Fig. 3b). GSDMD D275A also resisted cleavage by caspase-11 and caspase-4 in LPS-stimulated iBMDM and HeLa cells, respectively (Fig. 3a, c), and was unable to mediate LPS-induced pyroptosis (Fig. 3b, d).

In bacterial infection assays, complementation of the *Gsdmd*$^{-/-}$ iBMDMs with wild-type GSDMD restored *S. typhimurium*-induced pyroptosis but the D275A mutant showed no activity (Fig. 3e). While wild-type GSDMD was cleaved in the T3SS-dependent manner, the D275A mutant protein remained intact (Extended Data Fig. 8c). The same results were observed in *B. thailandensis* and enteropathogenic *Escherichia coli* infections (Fig. 3f and Extended Data Fig. 8d). In HeLa cell infection, *S. typhimurium* Δ*sifA* triggered caspase-4-dependent pyroptosis[9,14]. This cell death was diminished in *GSDMD*$^{-/-}$ cells (Fig. 3g). Notably, expression of wild-type GSDMD but not the D275A mutant in *GSDMD*$^{-/-}$ cells restored *S. typhimurium* Δ*sifA*-triggered pyroptosis (Fig. 3g).

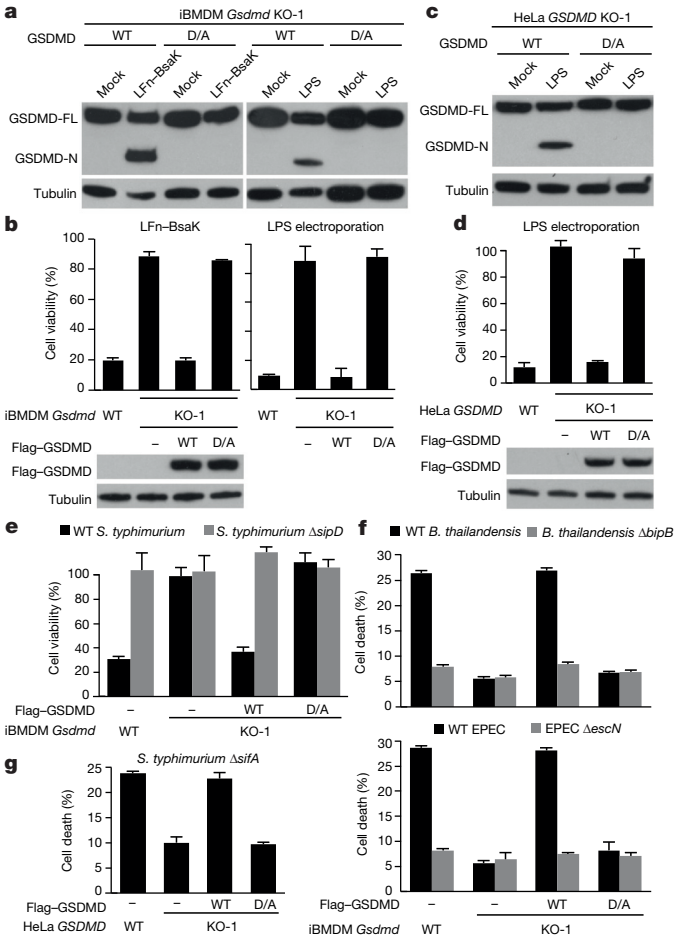

Figure 3 | Cleavage of GSDMD by inflammatory caspases is required for pyroptosis. **a**–**d**, Assays of the cleavage-resistant mutant of GSDMD in caspase-1 and caspase-4/11-mediated pyroptosis induced by LFn–BsaK and LPS electroporation, respectively. **e**–**g**, Assays of the cleavage-resistant mutant of GSDMD in bacterial-infection-induced pyroptosis. iBMDM cells were infected with wild-type *S. typhimurium* (**e**), *B. thailandensis* or enteropathogenic *E. coli* (EPEC) (**f**) or their T3SS-deficient mutants (Δ*sipD*, Δ*bipB* and Δ*escN*, respectively) as controls. HeLa cells were infected with *S. typhimurium* Δ*sifA* (**g**). The wild-type or the D275A mutants (D/A) of 2×Flag–HA–GSDMD (**a**, **c**) and Flag–GSDMD (**b**, **d**–**g**) were stably expressed in the knockout cells. Cell lysates were analysed by anti-Flag and anti-tubulin immunoblotting (**a**–**d**). Lysates of non-stimulated cells were analysed in **b** and **d**. ATP-based cell viability (**b**, **d**, **e**) and LDH-release-based cell death (**f**, **g**) are expressed as mean values ± s.d. from three technical replicates. All data shown are representative of three independent experiments.

Cleavage of GSDMD is sufficient to drive pyroptosis

To investigate whether cleavage at Asp275 in GSDMD is sufficient to initiate pyroptosis, a PreScission protease (PPase) recognition sequence (EVLFNGP) was inserted between Leu273 and Thr274 in the $_{272}$FLTD$_{275}$ motif in GSDMD. Expression of this engineered GSDMD(EVLFNGP) mutant or wild-type GSDMD in 293T cells by itself triggered no pyroptosis. However, upon cytosolic delivery of purified PPase, cells expressing GSDMD(EVLFNGP) but not wild-type GSDMD died extensively (Fig. 4a). Consistently, GSDMD(EVLFNGP) but not the wild-type protein was cleaved into the expected size by the PPase (Fig. 4b). The dying cells developed typical pyroptosis morphology with cell swelling and membrane rupture (Fig. 4a). We also

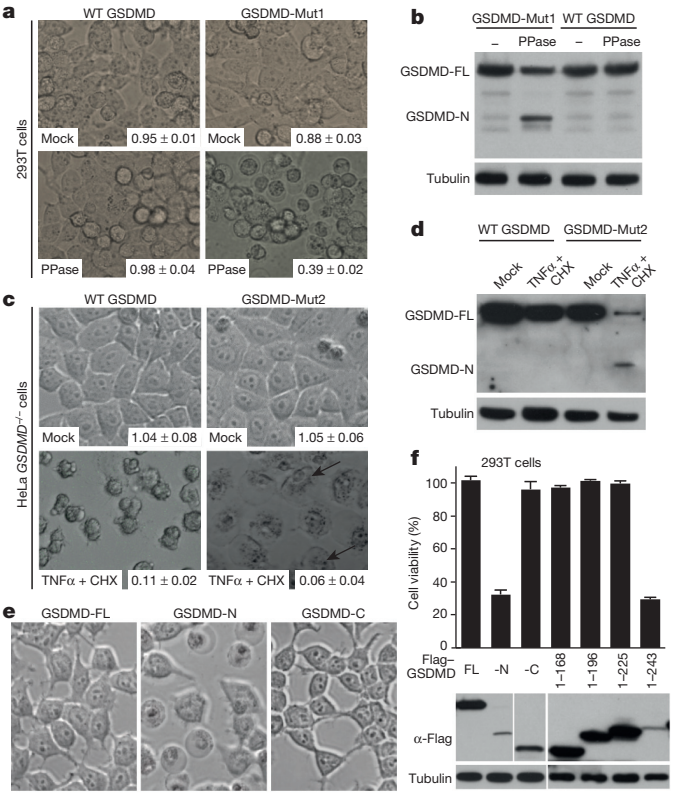

Figure 4 | Interdomain cleavage of GSDMD is sufficient to trigger pyroptosis owing to the intrinsic pyroptosis-inducing activity in its N-terminal domain. **a**, **b**, Pyroptosis induced by interdomain cleavage of an engineered GSDMD by PPase. 293T cells were transfected with Flag-tagged wild-type GSDMD or GSDMD-Mut1 (insertion of the PPase recognition sequence EVLFQGP into the FLTD site). Purified PPase was electroporated into the cells. **c**, **d**, Switch of TNFα-induced apoptosis to pyroptosis by the caspase-3-sensitive GSDMD mutant. Flag-tagged wild-type GSDMD or GSDMD-Mut2 (replacement of the FLTD motif with the caspase-3-cleavage site DEVD) was stably expressed in HeLa *GSDMD*$^{-/-}$ cells. Cells were treated with TNFα + CHX for 8 h. **e**, **f**, The pyroptosis-inducing activity of GSDMD N-terminal domain. Indicated GSDMD fragments were transiently expressed in 293T cells. GSDMD-FL, full-length GSDMD; GSDMD-N and GSDMD-C, the N- and C-terminal product of GSDMD generated by inflammatory caspase cleavage, respectively. Phase-contrast images of cell morphology are shown in **a**, **c** and **e**. ATP-based cell viability is expressed as mean values ± s.d. from three technical replicates (**a**, **c**, **f**) and are marked on the images in decimal form (**a**, **c**). Cell lysates were analysed by anti-Flag and anti-tubulin immunoblotting (**b**, **d**, **f**). All data shown are representative of three independent experiments.

engineered the FLTD site into DEVD, the cleavage site of caspase-3/7, and the resulting GSDMD(DEVD) mutant was stably expressed in *GSDMD*$^{-/-}$ HeLa cells. When stimulated with TNFα + CHX, both wild-type GSDMD and GSDMD(DEVD) mutant-expressing cells showed massive cell death (Fig. 4c). As expected, cells expressing wild-type GSDMD underwent apoptosis with no GSDMD cleavage. In contrast, GSDMD(DEVD) mutant-expressing cells showed typical pyroptotic morphology, in which the mutant GSDMD was proteolysed to the expected size by activated endogenous caspase-3/7 (Fig. 4c, d). The switch of TNFα-induced apoptosis to pyroptosis by the caspase-3/7-sensitive GSDMD(DEVD) can be observed in Supplementary Videos 1 and 2. These results establish that proteolytic cleavage at Asp275 in GSDMD is sufficient to instruct mammalian cells to undergo pyroptosis.

Pyroptosis-inducing activity of GSDMD-N domain

The function of GSDMD is completely unknown. *Gsdmd*$^{-/-}$ mice have no obvious phenotypes with normal epithelial differentiation in the intestinal tract despite high expression in gastrointestinal tracts[24]. To understand the functional mechanism of GSDMD cleavage in pyroptosis, the N-terminal and C-terminal cleavage fragments (GSDMD-N and GSDMD-C, respectively) were individually expressed in 293T cells. In contrast to GSDMD-C and full-length GSDMD, GSDMD-N could cause extensive cell death with apparent pyroptosis morphology (Fig. 4e, f). GSDMD-N was expressed at a much lower level than GSDMD-C and full-length GSDMD, a phenomenon commonly seen in proteins with cytotoxicity. Progressive truncations identified residues 1–243 of GSDMD as the minimal fragment capable of triggering pyroptosis (Fig. 4f).

Autoinhibition of GSDMD and the gasdermin family

Above analyses suggest that GSDMD-C may interact with GSDMD-N and this autoinhibition is released upon interdomain cleavage by inflammatory caspases. Supporting this idea, GSDMD-C was efficiently co-immunoprecipitated by GSDMD-N in transfected 293T cells (Fig. 5a). Furthermore, overexpression of GSDMD-C could block LPS-induced pyroptosis in HeLa cells due to *trans*-inhibition of endogenous GSDMD-N generated from caspase-4 cleavage (Fig. 5b).

GSDMD belongs to the gasdermin family that also contains GSDMA, GSDMB, GSDMC, DFNA5 and DFNB59 (Extended Data Fig. 2b)[25,26]. The gasdermin family shares ~ 45% overall sequence homology. Structures of the gasdermins can be divided into two domains, the gasdermin-N and -C domains, corresponding to the two cleavage fragments of GSDMD by inflammatory caspases (Fig. 2f). Mice lack *GsdmB*, but encode three GSDMA (GSDMA1–A3) and four GSDMC (GSDMC1–C4) proteins (Extended Data Fig. 2b). Other gasdermins do not share the FLTD motif in GSDMD (Extended Data Fig. 2a). Consistently, GSDMA, GSDMB and GSDMC resisted caspase-1/11 cleavage in 293T cells (Extended Data Fig. 9a). The gasdermin-N domain of GSDMA, GSDMB and GSDMC all could bind to its respective gasdermin-C domain (Fig. 5c), suggesting a similar autoinhibition that is released by mechanisms other than caspase cleavage.

Pyroptosis-inducing activity of GSDMA3 in disease

The function of the gasdermin family is poorly characterized[25,26]. GSDMA3 is the most studied gasdermin; mice with spontaneous or chemically induced mutations in *Gsdma3* exhibit hyperkeratosis and hair-loss phenotypes in the skin[25–27]. The mechanism for this alopecia pathology is unknown, but severe chronic inflammation has been observed in the skin of *Gsdma3*-mutant mice[28,29]. Like GSDMD, GSDMA3 exhibited the intramolecular interaction between its gasdermin-N and -C domains (Fig. 5c). Overexpression of the gasdermin-N domain of GSDMA3 (residues 1–284), but not full-length GSDMA3, caused extensive pyroptosis in 293T cells (Fig. 5d); GSDMA3 was not cleaved by inflammatory caspases but artificial interdomain cleavage of an engineered GSDMA3 by PPase could cause 293T cell pyroptosis (Extended Data Fig. 9b). GSDMA3 also remained intact in TNFα-induced apoptosis and necroptosis (Extended Data Fig. 9c). These data suggest that GSDMA3 is an autoinhibited pyroptosis-inducing factor functioning in an unknown biological process. The autoinhibition is partially supported by a recent intriguing study that proposes a function of GSDMA3 in autophagy[30].

Gsdma3$^{-/-}$ mice show no visible skin defects[30]. In fact, the hyperkeratosis and hair-loss phenotype in *Gsdma3*-mutant mice is dominant and the mutations are gain-of-function[25]. There are nine reported *Gsdma3* mutant alleles, resulting in 259RDW (insertion after residue 259 with mistranslated RDW sequence), T278P, L343P, Y344C, Y344H, A348T, I359N, premature stop at 366, and duplica-

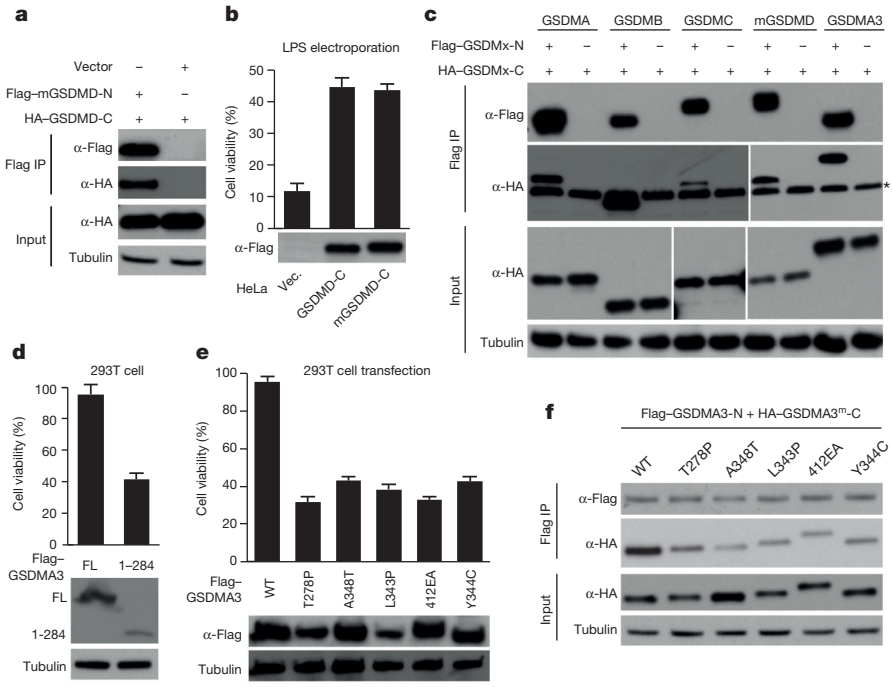

Figure 5 | Autoinhibition of the pyroptosis-inducing activity of the gasdermin family. **a**, **c**, Co-immunoprecipitation assay of the interaction between the gasdermin-N and -C domains in GSDMD and other gasdermin family members. * indicates antibody light chain. mGSDMD, mouse GSDMD. **b**, Effects of GSDMD-C domain overexpression on LPS electroporation-induced pyroptosis. Vec., vector. **d**, **e**, The pyroptosis-inducing activity of GSDMA3-N domain and its alopecia-causing mutants. **f**, Effects of the alopecia-causing mutations on the co-immunoprecipitation interaction between the N and C domains of GSDMA3. GSDMA3^{m}, point mutants of GSDMA3 analysed here. Indicated gasdermin constructs were expressed in 293T cells. Anti-Flag immunoprecipitation (**a**, **c**, **f**) was performed. The immunoprecipitates (Flag IP) or the total lysates were analysed by immunoblotting with antibodies against indicated epitopes or tubulin. ATP-based cell viability is expressed as mean values ± s.d. from three technical replicates (**b**, **d**, **e**). All data shown are representative of three independent experiments.

tion of E411A412 (412EA), in the gasdermin-C domain[25–27]. Five of the mutations (T278P, L343P, Y344C, A348T and 412EA) were analysed and found capable of instructing 293T cells to undergo pyroptosis (Fig. 5e). These mutations all disrupted or attenuated the co-immunoprecipitation between the gasdermin-N and -C domains of GSDMA3 (Fig. 5f). Thus, the alopecia-causing GSDMA3 mutants lose the autoinhibition and become constitutively active in triggering pyroptosis. Taken all together, our analyses further suggest that gasdermins are all pyroptosis-inducing factors that are activated by release of the autoinhibition on their gasdermin-N domains.

Discussion

We identify GSDMD as a generic substrate for caspase-1 and caspase-4/5/11. Cleavage of GSDMD by the inflammatory caspases critically determines pyroptosis by releasing the cleaved gasdermin-N domain that bears intrinsic pyroptosis-inducing activity. Further understanding the mechanism of action of GSDMD may provide a new avenue for therapeutic intervention of inflammatory-caspase-associated autoinflammatory conditions and septic shock. We also show that other gasdermins have a similar pyroptosis function; importantly, this observation redefines the concept of pyroptosis as gasdermin-mediated programmed necrosis.

Caspases are classified into apoptotic and inflammatory caspases. Substrate targeting by these caspases is known to be promiscuous to some extent; overlapping substrate spectra for caspases of different natures have been noted in proteomic efforts that identified GSDMD as a substrate for both caspase-1 and apoptotic caspases[31,32]. Our data suggest that interdomain cleavage of GSDMD by caspase-1/4/5/11 determines pyroptosis. Caspase-1 can also cleave caspase-3/7[21], which may have a pyroptosis-independent function, particularly in the absence of GSDMD. Thus, the substrate cleaved by a caspase in a cellular context is the determinant for the nature of the cell death. Pyroptosis and necroptosis are two types of lytic and programmed necrosis. In necroptosis, a pseudokinase MLKL, upon phosphorylation by RIPK3, acts as the executioner to rupture the membrane[22]. It is unclear at this stage whether GSDMD plays a similar 'executioner' role in pyroptosis, but our data suggest that GSDMD, or more specifically its gasdermin-N domain, is sufficient to drive pyroptosis regardless of the cellular system. Given the possible presence of other GSDMD- and MLKL-like necrosis factors, our results suggest a new paradigm for understanding programmed necrosis.

Online Content Methods, along with any additional Extended Data display items and Source Data, are available in the online version of the paper; references unique to these sections appear only in the online paper.

Received 23 June; accepted 25 August 2015.
Published online 16 September 2015.

1. Lamkanfi, M. & Dixit, V. M. Mechanisms and functions of inflammasomes. *Cell* **157,** 1013–1022 (2014).
2. Henao-Mejia, J., Elinav, E., Thaiss, C. A. & Flavell, R. A. Inflammasomes and metabolic disease. *Annu.Rev. Physiol.* **76,** 57–78 (2014).
3. Kofoed, E. M. & Vance, R. E. Innate immune recognition of bacterial ligands by NAIPs determines inflammasome specificity. *Nature* **477,** 592–595 (2011).
4. Zhao, Y. *et al.* The NLRC4 inflammasome receptors for bacterial flagellin and type III secretion apparatus. *Nature* **477,** 596–600 (2011).
5. Zhao, Y. & Shao, F. The NAIP-NLRC4 inflammasome in innate immune detection of bacterial flagellin and type III secretion apparatus. *Immunol.Rev.* **265,** 85–102 (2015).
6. Xu, H. *et al.* Innate immune sensing of bacterial modifications of Rho GTPases by the Pyrin inflammasome. *Nature* **513,** 237–241 (2014).
7. Kayagaki, N. *et al.* Noncanonical inflammasome activation by intracellular LPS independent of TLR4. *Science* **341,** 1246–1249 (2013).
8. Hagar, J. A., Powell, D. A., Aachoui, Y., Ernst, R. K. & Miao, E. A. Cytoplasmic LPS activates caspase-11: implications in TLR4-independent endotoxic shock. *Science* **341,** 1250–1253 (2013).
9. Shi, J. *et al.* Inflammatory caspases are innate immune receptors for intracellular LPS. *Nature* **514,** 187–192 (2014).
10. Yang, J., Zhao, Y. & Shao, F. Non-canonical activation of inflammatory caspases by cytosolic LPS in innate immunity. *Curr.Opin.Immunol.* **32,** 78–83 (2015).
11. Kayagaki, N. *et al.* Non-canonical inflammasome activation targets caspase-11. *Nature* **479,** 117–121 (2011).
12. Jorgensen, I. & Miao, E. A. Pyroptotic cell death defends against intracellular pathogens. *Immunol.Rev.* **265,** 130–142 (2015).
13. Miao, E. A. *et al.* Caspase-1-induced pyroptosis is an innate immune effector mechanism against intracellular bacteria. *Nature Immunol.* **11,** 1136–1142 (2010).
14. Aachoui, Y. *et al.* Caspase-11 protects against bacteria that escape the vacuole. *Science* **339,** 975–978 (2013).
15. Sauer, J. D. *et al.* Listeria monocytogenes engineered to activate the Nlrc4 inflammasome are severely attenuated and are poor inducers of protective immunity. *Proc. Natl Acad. Sci. USA* **108,** 12419–12424 (2011).
16. Kovarova, M. *et al.* NLRP1-dependent pyroptosis leads to acute lung injury and morbidity in mice. *J. Immunol.* **189,** 2006–2016 (2012).
17. Masters, S. L. *et al.* NLRP1 inflammasome activation induces pyroptosis of hematopoietic progenitor cells. *Immunity* **37,** 1009–1023 (2012).
18. Doitsh, G. *et al.* Cell death by pyroptosis drives CD4 T-cell depletion in HIV-1 infection. *Nature* **505,** 509–514 (2014).
19. von Moltke, J. *et al.* Rapid induction of inflammatory lipid mediators by the inflammasome *in vivo*. *Nature* **490,** 107–111 (2012).
20. Yang, J., Zhao, Y., Shi, J. & Shao, F. Human NAIP and mouse NAIP1 recognize bacterial type III secretion needle protein for inflammasome activation. *Proc. Natl Acad. Sci. USA* **110,** 14408–14413 (2013).
21. Akhter, A. *et al.* Caspase-7 activation by the Nlrc4/Ipaf inflammasome restricts *Legionella pneumophila* infection. *PLoSPathog.* **5,** e1000361 (2009).
22. Sun, L. & Wang, X. A new kind of cell suicide: mechanisms and functions of programmed necrosis. *Trends Biochem.Sci.* **39,** 587–593 (2014).
23. Poreba, M., Strozyk, A., Salvesen, G. S. & Drag, M. Caspase substrates and inhibitors. *Cold Spring Harb.Perspect.Biol.* **5,** a008680 (2013).
24. Fujii, T. *et al.* Gasdermin D (*Gsdmd*) is dispensable for mouse intestinal epithelium development. *Genesis* **46,** 418–423 (2008).
25. Tanaka, S., Mizushina, Y., Kato, Y., Tamura, M. & Shiroishi, T. Functional conservation of *Gsdma* cluster genes specifically duplicated in the mouse genome. *G3 (Bethesda)* **3,** 1843–1850 (2013).
26. Saeki, N. & Sasaki, H. in *Endothelium and epithelium: composition, functions, and pathology* (eds J. Carrasco & M. Matheus) Ch. IX 193–211 (Nova Science Publishers, 2011).
27. Kumar, S. *et al.* Gsdma3^{I359N} is a novel ENU-induced mutant mouse line for studying the function of Gasdermin A3 in the hair follicle and epidermis. *J. Dermatol. Sci.* **67,** 190–192 (2012).
28. Ruge, F. *et al.* Delineating immune-mediated mechanisms underlying hair follicle destruction in the mouse mutant defolliculated. *J. Invest. Dermatol.* **131,** 572–579 (2011).
29. Zhou, Y. *et al. Gsdma3* mutation causes bulge stem cell depletion and alopecia mediated by skin inflammation. *Am. J. Pathol.* **180,** 763–774 (2012).
30. Shi, P. *et al.* Loss of conserved *Gsdma3* self-regulation causes autophagy and cell death. *Biochem. J.* **468,** 325–336 (2015).
31. Agard, N. J., Maltby, D. & Wells, J. A. Inflammatory stimuli regulate caspase substrate profiles. *Mol. Cell. Proteomics* **9,** 880–893 (2010).
32. Crawford, E. D. *et al.* The DegraBase: a database of proteolysis in healthy and apoptotic human cells. *Mol. Cell. Proteomics* **12,** 813–824 (2013).

Supplementary Information is available in the online version of the paper.

Acknowledgements We thank J. Ding for recombinant protein purification and X. Wang for reagents. We thank members of the Shao laboratory for helpful discussions and technical assistance. This work was supported by the Strategic Priority Research Program of the Chinese Academy of Sciences (XDB08020202), the China National Science Foundation Program for Distinguished Young Scholars (31225002) and Program for International Collaborations (31461143006), and the National Basic Research Program of China 973 Program (2012CB518700 and 2014CB849602) to F.S. The research was supported in part by an International Early Career Scientist grant from the Howard Hughes Medical Institute and the Beijing Scholar Program to F.S.

Author Contributions F.S. and J.S. conceived the study; J.S. performed the CRISPR-Cas9 screens; J.S. and Y.Zha. designed and performed the majority of experiments, assisted by K.W. and X. S.; H.H. and T.C. performed the deep sequencing; J.S., Y.W., Y.Zhu. and F.W. generated the knockout mice. J.S., Y.Zha. and F.S. analysed the data and wrote the manuscript. All authors discussed the results and commented on the manuscript.

Author Information Reprints and permissions information is available at www.nature.com/reprints. The authors declare no competing financial interests. Readers are welcome to comment on the online version of the paper. Correspondence and requests for materials should be addressed to F.S. (shaofeng@nibs.ac.cn).

METHODS

No statistical methods were used to predetermine sample size. The experiments were not randomized and the investigators were not blinded to allocation during experiments and outcome assessment.

Plasmids, antibodies and reagents. Complementary DNA (cDNA) for human *GSDMD* was amplified from reverse-transcribed cDNA of HT-29 cells; cDNAs for human *GSDMB*, human *GSDMC* and mouse *Gsdma3* were synthesized by our in-house gene synthesis facility; cDNAs for human *GSDMA* and mouse *Gsdmd* were obtained from Vigene Biosciences (CH892815) and OriGene (MC202215), respectively. The gasdermin cDNAs were inserted into a modified pCS2-3×Flag vector for transient expression in 293T cells and the pWPI lentiviral vector with an N-terminal 2×Flag–HA tag or the FUIGW vector with an N-terminal Flag tag for stable expression in HeLa and iBMDM cells. For recombinant expression in *E. coli*, the cDNAs were cloned into a modified pET vector with an N-terminal SUMO tag. Truncation mutants of the gasdermins were constructed by the standard PCR cloning strategy and inserted into the pCS2 vector with indicated tags. Expression plasmids for caspase-1, 4, 5 and 11 were previously described[4,9], the caspase-9 plasmid was a gift from X. Wang (National Institute of Biological Sciences, Beijing). cDNAs for human *CASP2* and mouse *Casp8* are from the Life Technologies Ultimate ORF collection and OriGene (MC200404), respectively. Point mutations were generated by the QuickChange Site-Directed Mutagenesis Kit (Stratagene). All plasmids were verified by DNA sequencing.

Antibodies for caspase-1 p10 (sc-515), Myc epitope (sc-789) and GSDMD (sc-81868) were obtained from Santa Cruz Biotechnology. Other antibodies used in this study include anti-HA (MMS-101P, Covance), anti-Flag M2 (F4049), anti-actin (A2066) and anti-tubulin (T5168) (Sigma-Aldrich), rat monoclonal caspase-11 17D9 (NB120-10454, Novus Biologicals), anti-caspase-3 (#9662) and caspase-7 (#12827) (Cell Signaling Technology), IL-1β (3ZD; Biological Resources Branch, National Cancer Institute) and the antibody for detecting endogenous GSDMD (NBP2-33422, Novus Biologicals). Ultrapure LPS from *E. coli* O111:B4 and poly(dA:dT) were purchased from InvivoGen. LPS (L4524, for priming), TNFα and cycloheximide were purchased from Sigma-Aldrich. SMAC mimetic and the pan-caspase inhibitor zVAD are gifts from the laboratory of X. Wang (National Institute of Biological Sciences, Beijing). Nigericin was purchased from Calbiochem. Recombinant p20/p10 active caspase proteins (caspase-1/2/4/8/9) and lipid A (ALX-581-200-L001) were obtained from Enzo Life Sciences. Cell culture products are from Life technologies and all other chemicals used are Sigma-Aldrich products unless noted.

Cell culture and transfection. HeLa, HT-29 and 293T cells were obtained from ATCC. C57BL/6 mice-derived wild-type and *Tlr4*$^{-/-}$iBMDM cells were kindly provided by K. A. Fitzgerald (University of Massachusetts Medical School, United States) and A. Ding (Weill Cornell Medical College, United States), respectively, and used in our previous studies[4,6,30]. All the cell lines are well-established, commonly used and frequently checked by virtue of their morphological features and functionalities, but have not been subjected to authentication by short tandem repeat (STR) profiling. All the cell lines have been tested to be mycoplasma-negative by the commonly used PCR method. iBMDM, HeLa and 293T cells were grown in Dulbecco's modified Eagle's medium (DMEM); HT-29 cells were grown in McCoy's 5a modified medium. All media were supplemented with 10% (vol/vol) fetal bovine serum (FBS) and 2 mM L-glutamine. All cells were grown at 37 °C in a 5% CO_2 incubator. Transient transfection of HeLa and 293T cells was performed using the JetPRIME (Polyplus Transfection) or Vigofect (Vigorous) reagents by following the manufacturers' instructions. For stable expression, lentiviral plasmids harbouring the desired gene were first transfected into 293T cells together with the packing plasmids pSPAX2 and pMD2G with a ratio of 5:3:2. The supernatants were collected 48 h after transfection and used to infect HeLa or iBMDM cells for another 48 h. GFP-positive infected cells were sorted by flow cytometry (BD Biosciences FACSAria II). For siRNA knockdown, 0.5 μl of 20 μM siRNA together with 0.8 μl of INTERFERin reagents (Polyplus Transfection) were used for reverse transfection of iBMDM cells in the 96-well plate format; 5 μl of 20 μM siRNA and 10 μl of INTERFERin reagents were used to transfect HeLa cells in the 6-well plate format. The knockdown was performed for 60 h before subsequent analyses. The knockdown efficiency was assessed by quantitative real-time PCR (qRT–PCR) analyses as previously described[4]. All siRNA oligonucleotides were synthesized by our in-house facility using the sequences from the MISSION shRNA library (Broad Institute, United States) and their sequences are listed in Supplementary Table 1.

Inflammasome activation assays. Activation of the canonical caspase-1 inflammasomes (the NLRP3, NAIP–NLRC4 and AIM2 inflammasomes) and the non-canonical caspase-11 inflammasome by LPS was performed using the protocols that have been detailed in our previous publications[4,6,9,20]. For bacteria-induced inflammasome activation, *S. typhimurium* (wild-type and Δ*sipD*), *B. thailandensis* (wild-type and Δ*bipB*), EPEC (wild-type and Δ*escN*) were used to infect iBMDM cells and *S. typhimurium* (wild-type and Δ*sifA*) was used to infect HeLa cells, as described previously[4,9].

Microscopy imaging of cell death. To examine cell death morphology, cells were treated as indicated in the 6-well plates (Nunc products, Thermo Fisher Scientific Inc.) for static image capture or in glass-bottom culture dishes (MatTek Corporation) for live imaging. Static bright field images of pyroptotic cells were captured using an Olympus IX71 or a Zeiss Pascal Confocal microscope. The image pictures were processed using ImageJ or the LSM Image Examiner program. Live images of cell death were recorded with the PerkinElmer UltraVIEW spinning disk confocal microscopy and processed in the software Volocity. All image data shown were representative of at least three randomly selected fields.

Genome-wide CRISPR-Cas9 screens. The lentiviral gRNA plasmid library for genome-wide CRISPR-Cas9 screen was obtained from Addgene (#50947)[33]; amplification of the library and preparation of the lentivirus were performed following the protocol provided by Addgene. In brief, 1 μl of library DNA (10 ng μl^{-1}) was used to transform 25 μl of electrocompetent *E. coli* (TaKaRa). Transformed colonies (>6×10^7) were scraped off the Luria-Bertani (LB) plates into the media, and plasmids were exacted by using the GoldHi EndoFree Plasmid Maxi Kit (CWBIO). To prepare the virus library, 293T cells in the 15-cm dish were transfected with 25 μg of library DNA together with 15 μg of psPAX2 and 10 μg of pMD2.G. Eight hours after transfection, the media were changed to high-serum DMEM (20% FBS with 25 mM HEPES). Another 40 h later, the media (from twenty 15-cm dishes of transfected cells) were collected and centrifuged at 3,000 r.p.m. for 10 min. The supernatant was filtered through a 0.22-μm membrane and aliquots of 30 ml were stored at −80 °C.

In the pilot experiment, the volume of the lentivirus library required for achieving an MOI of 0.3 for infecting the target cell line was determined in the 12-well plate format. For the large scale screen, *Tlr4*$^{-/-}$ iBMDM cells stably expressing the Cas9 protein were seeded in the 15-cm dish (2×10^6 cells in 20 ml media per dish) and a total of 2×10^7 cells were infected with the gRNA lentivirus library. Sixty hours after infection, cells were re-seeded at a density of 1×10^5 ml^{-1} in fresh media supplemented with 5 μg ml^{-1}puromycin (to eliminate non-infected cells). After 6 to 8 days, ~3×10^8 cells from five culture dishes were electroporated with LPS to trigger caspase-11-mediated pyroptosis[9], or stimulated with LFn–BsaK/protective antigen (PA) to induce caspase-1-mediated pyroptosis[4]; another 3×10^8 cells were left untreated as the control sample. Each screen was repeated another time. Surviving cells were collected after growing to near 90% confluence and lysed in the SNET buffer (20 mM Tris-HCL(pH 8.0), 5 mM EDTA, 400 mM NaCl, 400 μg ml^{-1} Proteinase K and 1% SDS). Genomic DNAs of each group of cells were prepared by using the phenol-chloroform extraction and isopropanol precipitation method. The DNA was dissolved in H_2O (4–5 μg μl^{-1}) and used as the templates for amplification of the gRNA.

The gRNAs were amplified by a two-step PCR method using the Titanium Taq DNA polymerase (Clontech Laboratories). In the first step, six 50-μl PCR reactions (each containing 50 μg of genomic DNA template) were performed with the forward primer 50bp-F and the reverse primer 50bp-R; the PCR program used is 94 °C for 180 s, 16 cycles of 94 °C for 30 s, 60 °C for 10 s and 72 °C for 25 s, and a final 2-min extension at 68 °C. Products of the first-step PCR were pooled together and used as the template for the second-step PCR. Also six 50-μl PCR reactions (each containing 1 μl of the first-step PCR product) were performed with the forward primer Index-F and one of the reverse primers (Index-R1 to R6): Index-R1 for the control sample, Index-R2 for the replicate control sample, Index-R3 for the caspase-11 screen, Index-R4 for the replicate caspase-11 screen, Index-R5 for the caspase-1 screen and Index-R6 for the replicate caspase-1 screen. The PCR program used is 94 °C for 180 s, 18 cycles of 94 °C for 30 s, 54 °C for 10 s and 72 °C for 18 s, and a final 2-min extension at 68 °C. Products of the second-step PCR reactions were subjected to electrophoresis on the 1.5% agarose gel; the DNAs (the 310-bp band) were extracted and sequenced at the HiSeq2500 instrument (Illumina) by using the 50-bp single-end sequencing protocol. The first 19 nucleotides from each sequencing read are the gRNA sequence recovered from the library. The frequency of each gRNA was obtained by dividing the gRNA read number by the total sample read number; the fold of enrichment was calculated by comparing the frequency of each gRNA in the experiment sample with that in the control sample. Sequences for all the primers are listed in Supplementary Table 1.

The top 50 gRNA hits from the caspase-11 screen were examined and 18 genes that are conserved in human and mouse were identified for siRNA knockdown validation in HeLa cells. HeLa cells expressed caspase-4 but not caspase-5 (Extended Data Fig. 1b) and respond robustly to cytosolic LPS[9,10]. For each gene, a mixture of two independent siRNAs was used and the knockdown efficiency of 12 of those having mRNA expression in HeLa cells was confirmed. Importantly, only siRNAs targeting human *GSDMD*, besides the control *CASP4*-targeting

siRNA, could efficiently block cytosolic LPS-induced pyroptosis (Extended Data Fig. 1c). When assayed individually, the two *GSDMD*-targeting siRNAs both showed potent inhibition of HeLa cell pyroptosis (Extended Data Fig. 1d).

Generation of CRISPR-Cas9 knockout cell lines. Human codon-optimized Cas9 (hCas9) and GFP-targeting gRNA-expressing plasmids (gRNA_GFP-T1) were purchased from Addgene. The 19-bp GFP-targeting sequence in the gRNA vector was replaced with the sequence targeting the desired gene by QuickChange site-directed mutagenesis. The target sequences used are AGCATCCTGGC ATTCCGAG for mouse *Gsdmd* and TTCCACTTCTACGATGCCA for human *GSDMD*. To construct the knockout cell lines, 1 μg of gRNA-expressing plasmid, 3 μg of hCas9 plasmid and 1 μg of pEGFP-C1 vector were co-transfected into 6×10^6 iBMDM or HeLa cells. Three days later, GFP-positive cells were sorted into single clones into the 96-well plate by flow cytometry using the BD Biosciences FACSAria II or the Beckman Coulter MoFlo XDP cell sorter. Single clones were screened by the T7 endonuclease I-cutting assay and the candidate knockout clones were verified by sequencing of the PCR fragments as described previously[9]. The PCR primers used are listed in Supplementary Table 1.

Knockout mice and primary BMDM cells. All animal experiments were conducted following the Ministry of Health national guidelines for housing and care of laboratory animals and performed in accordance with institutional regulations after review and approval by the Institutional Animal Care and Use Committee at National Institute of Biological Sciences. The *Gsdmd* knockout mice were generated by co-microinjection of *in vitro*-translated *Cas9* mRNA and gRNA into the C57BL/6 zygotes. Founders with frameshift mutations were screened with T7E1 assay and validated by DNA sequencing. Founders were intercrossed to generate biallelic $Gsdmd^{-/-}$ mice. The gRNA sequence used to generate the knockout mice is AGCATCCTGGCATTCCGAG. C57BL/6 wild-type mice were from Vital River Laboratory Animal Technology Co. and $Casp1/11^{-/-}$ mice were obtained from the Jackson Laboratory. $Ripk3^{-/-}$ mice were a gift from X. Wang (National Institute of Biological Sciences, Beijing). Primary BMDM cells were prepared from 6-week-old male mice (C57BL/6 background) by following a standard procedure as previously described[6]. For each experimental design, at least two mice were chosen to prepare the BMDM cells for assaying the inflammasome responses; the mice were not randomized and the investigators were not blinded.

Cytotoxicity assay and IL-1β ELISA. Relevant cells were treated as indicated. Cell death was measured by the LDH assay using CytoTox 96 Non-Radioactive Cytotoxicity Assay kit (Promega). Cell viability was determined by the CellTiter-Glo Luminescent Cell Viability Assay (Promega). To measure IL-1β release, primary BMDM cells were primed with LPS (1 μg ml^{-1}) for 2 h and released mature IL-1β was determined by using the IL-1β ELISA kit (Neobioscience Technology Company).

Purification of recombinant proteins. To obtain recombinant human GSDMD, *E. coli* BL21 (DE3) cells harbouring pET28a-His_6-SUMO-GSDMD were grown in LB medium supplemented with 30 μg ml^{-1} kanamycin. Protein expression was induced overnight at 18 °C with 0.4 mM isopropyl-B-D-thiogalactopyranoside (IPTG) after $OD_{600\ nm}$ reached 0.8. Cells were harvested and resuspended in a lysis buffer containing 20 mM Tris-HCl (pH 8.0), 150 mM NaCl, 20 mM imidazole and 10 mM 2-mercaptoethanol. The His_6-SUMO-tagged protein was first purified by affinity chromatography using Ni-NTA beads (Qiagen) and the SUMO tag was removed by overnight ULP1 protease digestion at 4 °C. The cleaved GSDMD was further purified by HiTrap Q ion-exchange and Superdex G200 gel-filtration chromatography (GE Healthcare Life Sciences).

To obtain the constitutive-active caspase-11 p20/p10 tetramer, cDNAs encoding the p20 large and p10 small subunit were cloned into pET21a with a 6×His tag fused to the C terminus of the p10 subunit. The two subunits were separately expressed in *E. coli* with 1 mM IPTG induction for 4 h at 30 °C. Bacteria collected from 1-l culture were resuspended and lysed in 100 ml of lysis buffer (50 mM Tris-HCl (pH 8.0), 150 mM NaCl and 10 mM 2-mercaptoethanol) by sonication. Inclusion bodies, obtained by centrifugation of the lysates at 18,000 r.p.m. for 1 h, was washed with 50 ml of Buffer 1 (50 mM Tris-HCl (pH 8.0), 300 mM NaCl, 1 M guanidinium hydrochloride (GdnCl) and 0.1% Triton X-100) and 50 ml of Buffer 2 (50 mM Tris-HCl (pH 8.0), 300 mM NaCl and 1 M GdnCl) twice for each buffer. The washed inclusion bodies were solubilized by stirring in 6 ml of the solubilization buffer containing 6.5 M GdnCl, 25 mM Tris-HCl (pH 7.5), 5 mM EDTA and 100 mM DTT overnight at room temperature. To obtain active p20/p10 tetramers by refolding, 12 ml of above solubilized inclusion body solution containing denatured large and small subunits (molecular ratio, 1:2) were drop-by-drop diluted in 500 ml of refolding buffer (100 mM HEPES, 100 mM NaCl, 100 mM sodium malonate, 20% sucrose, 0.1 M NDSB-201 and 10 mM DTT) and then gently stirred in a nitrogen atmosphere at 16 °C overnight. Protein aggregates were removed by centrifugation at 4,000 r.p.m. for 20 min and the refolded protein supernatants were concentrated and dialysed against a buffer containing 50 mM Tris-HCl (pH 8.0), 150 mM NaCl and 10 mM 2-mercaptoethanol. The protein was affinity-purified by the Ni-NTA beads and further purified by the Superdex G200 gel-filtration chromatography. Expression and purification of recombinant LFn–BsaK and LFn–FliC proteins were described previously[4]. Recombinant full-length caspase-4 and caspase-11 were expressed and purified from insect cells also as previously described[9]. Recombinant PreScission protease (PPase) proteins are routine lab stocks.

***In vitro* GSDMD cleavage by recombinant caspases.** For cleavage by the p20/p10 tetramers of active caspase, 5 μg of purified recombinant GSDMD was incubated with 1 unit of caspase-1, 2, 4, 8 and 9 or 0.1 μg of caspase-11 in a 25-μl reaction containing 50 mM HEPES (pH 7.5), 3 mM EDTA, 150 mM NaCl, 0.005% (vol/vol) Tween-20 and 10 mM DTT. The reaction was incubated for 60 min at 37 °C. For cleavage by LPS-activated caspase-4/11, the full-length caspase proteins purified from insect cells were first incubated with LPS, lipid A or MDP for 30 min at 30 °C; 5 μg of purified recombinant GSDMD was then reacted with the ligand-incubated caspases at 37 °C for 9 min. Cleavage of GSDMD was examined by Coomassie blue staining of the reaction samples separated on the SDS–PAGE gel.

33. Koike-Yusa, H., Li, Y., Tan, E.-P., del Castillo Velasco-Herrera, M. & Yusa, K. Genome-wide recessive genetic screening in mammalian cells with a lentiviral CRISPR-guide RNA library. *Nature Biotechnol.* **32,** 267–273 (2014).

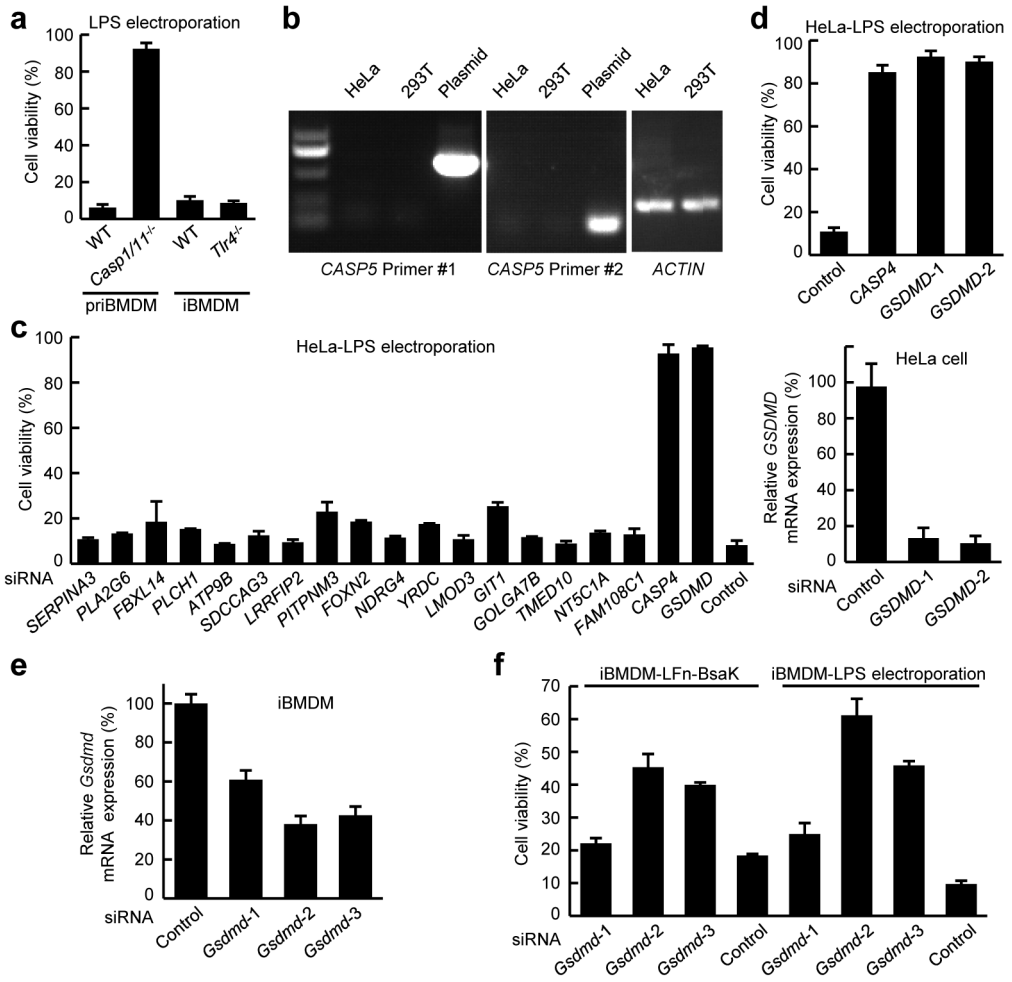

Extended Data Figure 1 | siRNA knockdown validation of the requirement of GSDMD for LPS- and LFn–BsaK-induced pyroptosis. **a**, LPS electroporation-induced pyroptosis in the absence of priming. Primary BMDMs (priBMDM) (wild-type (WT) or the *Casp1* and *Casp11* double knockout) or iBMDM cells (wild-type or $Tlr4^{-/-}$) were assayed. $Tlr4^{-/-}$ iBMDMs were used for the CRISPR-Cas9 screen in this study. **b**, Reverse-transcription PCR analyses of caspase-5 expression in HeLa and 293T cells. Plasmid harbouring caspase-5 cDNA serves as the positive control. **c**, siRNA knockdown validation of the CRISPR-Cas9 screen of LPS-induced pyroptosis. HeLa cells were used to validate the selected top hits from the screen. Mixtures of two independent siRNA pairs targeting each gene were transfected into the cells. siRNAs targeting *CASP4* and luciferase were used as the positive and negative control, respectively. **d**, Effects of *GSDMD* siRNA knockdown on LPS-induced pyroptosis in HeLa cells. **e**, **f**, Effects of *Gsdmd* siRNA knockdown on LPS and LFn–BsaK-induced pyroptosis in iBMDM cells. The knockdown efficiency (**d**, **e**) was measured by qRT–PCR analyses. ATP-based cell viability (**a**, **c**, **d**, **f**) and siRNA knockdown efficiency (**d**, **e**) were expressed as mean values ± s.d. from three technical replicates. Data shown are representative of two (**c**) or three (**a**, **b**, **d**–**f**) independent experiments.

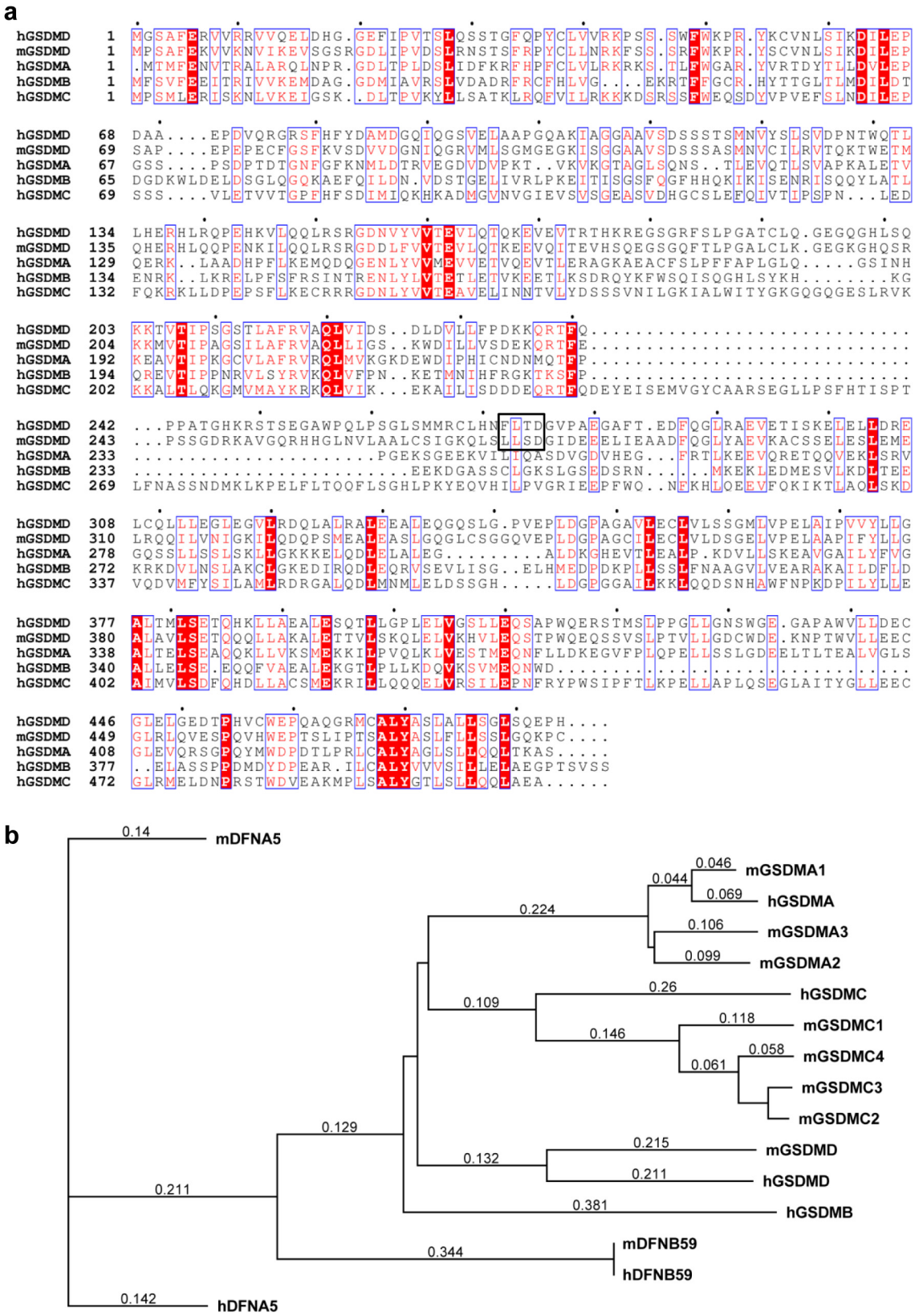

Extended Data Figure 2 | The gasdermin family of proteins in human and mouse. a, Multiple sequence alignment of human GSDMA, GSDMB, GSDMC, GSDMD and mouse GSDMD. The alignment was performed by using the ClustalW2 algorithm and displayed with ESPript 3.0 (http://espript.ibcp.fr/ESPript/cgi-bin/ESPript.cgi). Identical residues are highlighted by the dark red background and conserved residues are indicated by red font. The black box marks the caspase-1/4/11 cleavage motifs in human and mouse GSDMD. The residue number is indicated on the left of the sequence. **b**, Phylogenetic tree of all the gasdermin family of proteins in human and mouse. ClustalW alignment was carried out to generate the phylogenetic tree by using the 'Neighbor Joining' method. DFNA5 and DFNB59 are distantly related to the gasdermins, and the latter only contains gasdermin-N domain.

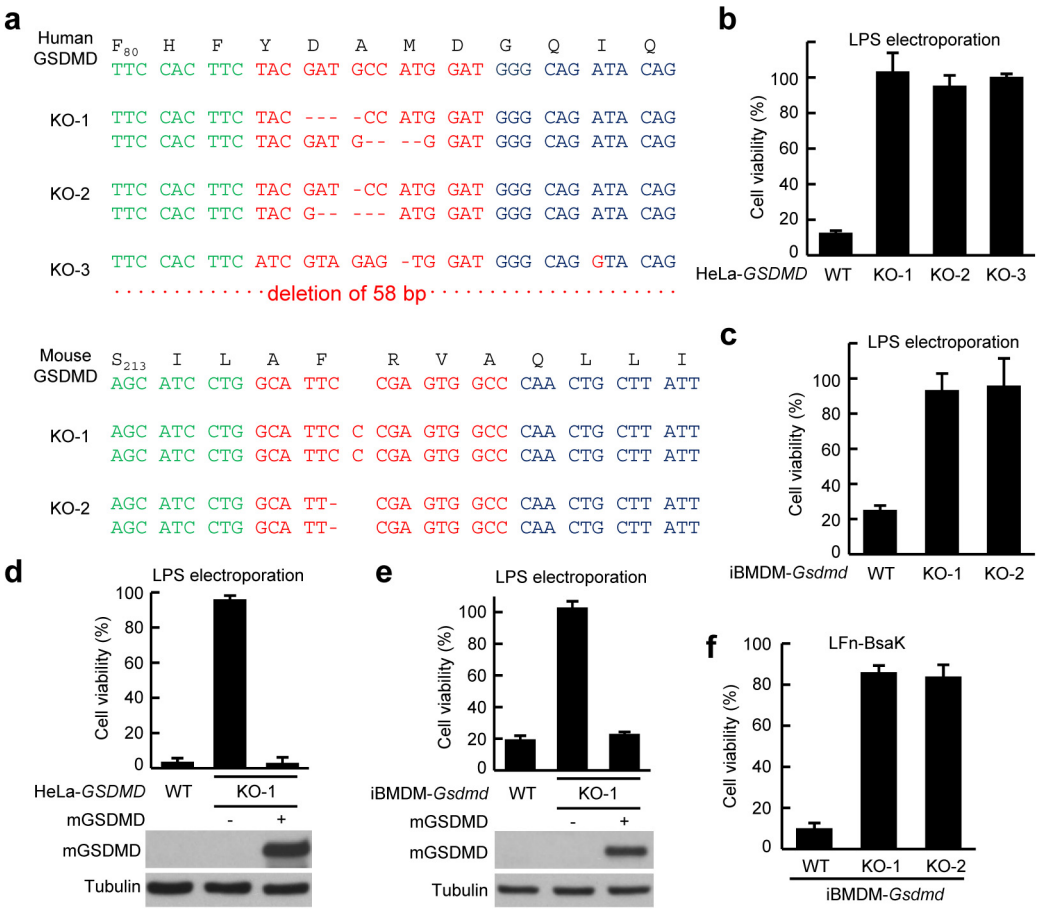

Extended Data Figure 3 | Generation of GSDMD-deficient cell lines and assays for cytosolic LPS- and LFn–BsaK-triggered pyroptosis. **a**, Generation of *GSDMD*$^{-/-}$ HeLa cells and *Gsdmd*$^{-/-}$ iBMDM cells by CRISPR-Cas9-mediated targeting. Shown are the sequence mutations of the three HeLa cell clones and two iBMDM clones used in the study. **b**, **c**, **f**, Effects of *GSDMD*$^{-/-}$ on LPS electroporation-induced pyroptosis in HeLa (**b**) and iBMDM cells (**c**) and LFn–BsaK-induced pyroptosis in iBMDM cells (**f**). **d**, **e**, Complementation of *GSDMD*$^{-/-}$ HeLa cells and *Gsdmd*$^{-/-}$ iBMDM cells by stably expressed mouse GSDMD–3×Flag. The accompanying blots show the expression of exogenous GSDMD by anti-Flag immunoblotting with anti-tubulin blots serving as the loading control. ATP-based cell viability is expressed as mean values ± s.d. from three technical replicates (**b**–**f**). Data shown are representative of at least three independent experiments.

a LFn-BsaK CRISPR-Cas9 screen hits with multiple gRNAs

Ranking	Gene_gRNA #	Average folds of enrichment	gRNA sequence
1	*Nlrc4_2*	3695.249	GTTTCGAATAGTCCCCCCC
2	*Nlrc4_1*	2797.553	AGGTGCCTCATGACCGCCC
3	*Nlrc4_5*	2202.819	ATATGGATGATCTTTCGGG
4	*Nlrc4_4*	1798.824	ATCAGCAAGCCGACCTTCA
6	*Naip2_5*	1599.965	TTCTGGTCGTAATTTCTTG
7	*Nlrc4_3*	1241.855	ATCTGCTCCTCTACACGTG
8	*Casp1_3*	1143.169	AGGGCAAGACGTGTACGAG
10	*Casp1_1*	877.4373	GAATTCTGGAGCTTCAATC
12	*Fbxo44_1*	659.6165	ATCGCCTCCGTTCACGTCC
13	*Casp1_5*	649.6994	ATGTCTCATGGTATCCAGG
15	*Naip2_4*	554.2724	ACTGGCCCCACGAATCACC
17	*Naip2_2*	315.3426	ACAGCCCCGGGTGATTCGT
18	*Casp1_4*	246.0405	CAACTTGAGCTCCAACCCT
21	*Naip2_1*	202.6801	CTAGACTCGTATCTAGGTA
36	*Antxr2_4*	67.18251	TGACGGACGGTAAGCTGGA
57	*Ccdc6_3*	35.80221	CTCGCCGTGAATTACGAGA
88	*Ccdc6_5*	23.54041	CTCGCCGTGAATTACGAGA
138	***Gsdmd_3***	16.5958	CAACAGCTTCGGAGTCGTG
153	*1700034J05Rik_4*	15.40841	CTCTTCAGGAAACGAGATC
171	*Plekhg6_3*	14.6932	CAGACCATGGCTTATGCGC
195	*Bcl2l2_1*	13.87979	CCTAACTGGGGCCGTCTTG
203	*Plekhg6_1*	13.46514	ATAAATGGCCAGGTCCGAC
236	*Fbxo44_4*	12.63271	GGCTTCATCACCGAGGACT
239	*Antxr2_2*	12.47934	GCTAGTGTTTACTGCGTTG
338	*Bcl2l2_5*	9.98516	CCTAACTGGGGCCGTCTTG
340	*1700034J05Rik_2*	9.970983	CTGGCCTGGGATATCGATG
352	***Gsdmd_4***	9.753432	AGCATCCTGGCATTCCGAG
353	*Gm97_5*	9.727808	CTGGCTCACCTATATGCCC
365	*Gm97_4*	9.490875	CTGGCTCACCTATATGCCC
376	*Ppp1r3b_3*	9.245637	AGCCCCTGGTTGTCGGCGA
380	*Ppp1r3b_5*	9.168484	ACAGTTTTCTAGGCAGACG

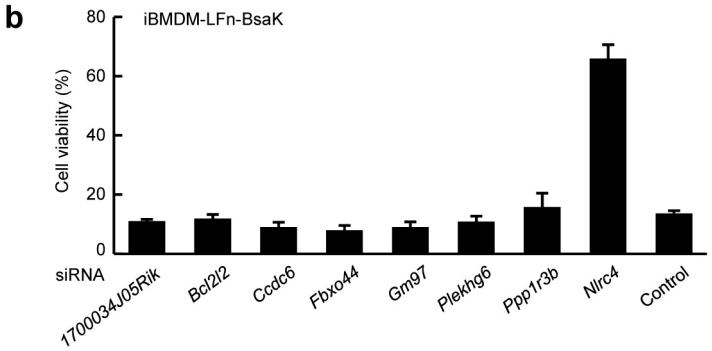

Extended Data Figure 4 | CRISPR-Cas9 screen of LFn–BsaK-triggered pyroptosis and effects of *Gsdmd* knockout on LFn–BsaK-induced and caspase-1-mediated caspase-3/7 cleavage. **a**, gRNA hits from a genome-wide CRISPR-Cas9 screen of LFn–BsaK-induced pyroptosis in mouse *Tlr4*$^{-/-}$ iBMDM cells. Shown are those genes with multiple gRNA hits. The ranking, the average fold increase and the sequences for each gRNA are listed. Genes highlighted in red encode known components in the pathway (*Antxr2* encodes the endocytosis receptor for the LFn tag) and were hit by multiple gRNAs. **b**, siRNA knockdown validation of screen hits. Mixtures of two independent siRNA pairs targeting each gene were transfected into the iBMDM cells before stimulation with LFn–BsaK. siRNAs targeting *Nlrc4* and luciferase were used as the positive and negative control, respectively. ATP-based cell viability is expressed as mean values ± s.d. from three technical replicates. **c**, Caspase-3/7 activation upon prolonged LFn–BsaK treatment in wild-type and *Gsdmd*$^{-/-}$ (the KO-1 clone; KO, knockout) iBMDM cells. Cell lysates were analysed by anti-caspase-3/7 and tubulin immunoblotting. Data shown are representative of two (**b**) and three (**c**) independent experiments.

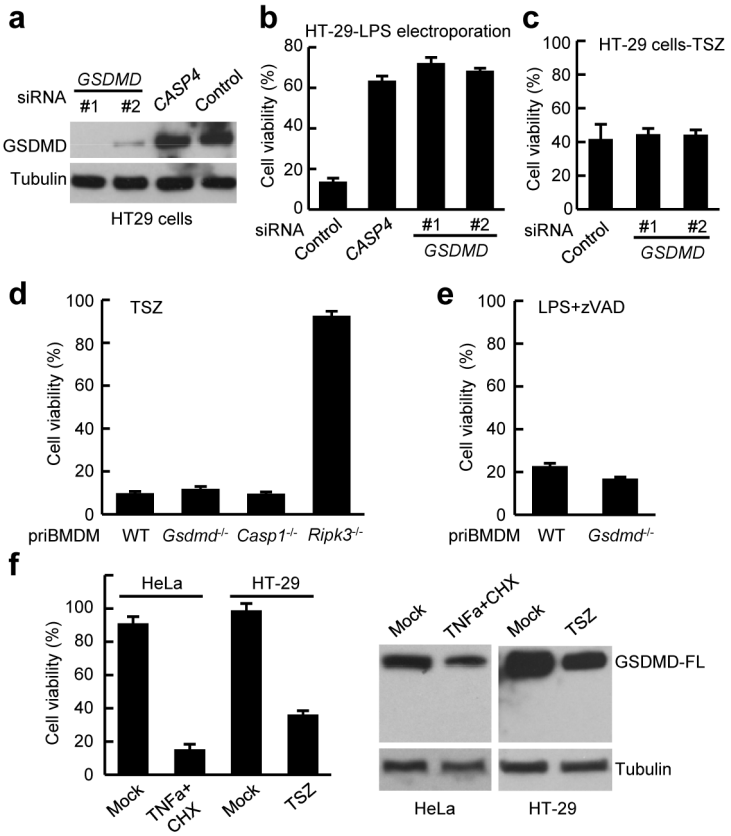

Extended Data Figure 5 | GSDMD is not required for and not cleaved in TNFα-induced necroptosis and apoptosis. **a**–**c**, Effects of *GSDMD* knockdown on LPS electroporation-induced pyroptosis and TSZ-induced necroptosis in HT-29 cells. Two independent *GSDMD*-targeting siRNAs (#1 and #2) were assayed and the immunoblots in **a** show the knockdown efficiency. **d**, **e**, Primary BMDM cells from *Gsdmd*$^{-/-}$ or other indicated mouse strains were stimulated with TSZ (**d**) or LPS + zVAD (**e**) to trigger necroptosis. **f**, The absence of GSDMD cleavage in TNFα-induced apoptosis and necroptosis. 2×Flag–HA–GSDMD was stably expressed in HeLa and HT-29 cells. Apoptosis was induced by TNFα + CHX treatment in HeLa cells and necroptosis was induced by TSZ stimulation of HT-29 cells. Lysates of stimulated cells were analysed by anti-Flag and anti-tubulin immunoblotting to examine possible GSDMD cleavage. GSDMD-FL, full-length GSDMD. ATP-based cell viability is expressed as mean values ± s.d. from three technical replicates (**b**–**f**). Data shown are representative of at least two independent experiments.

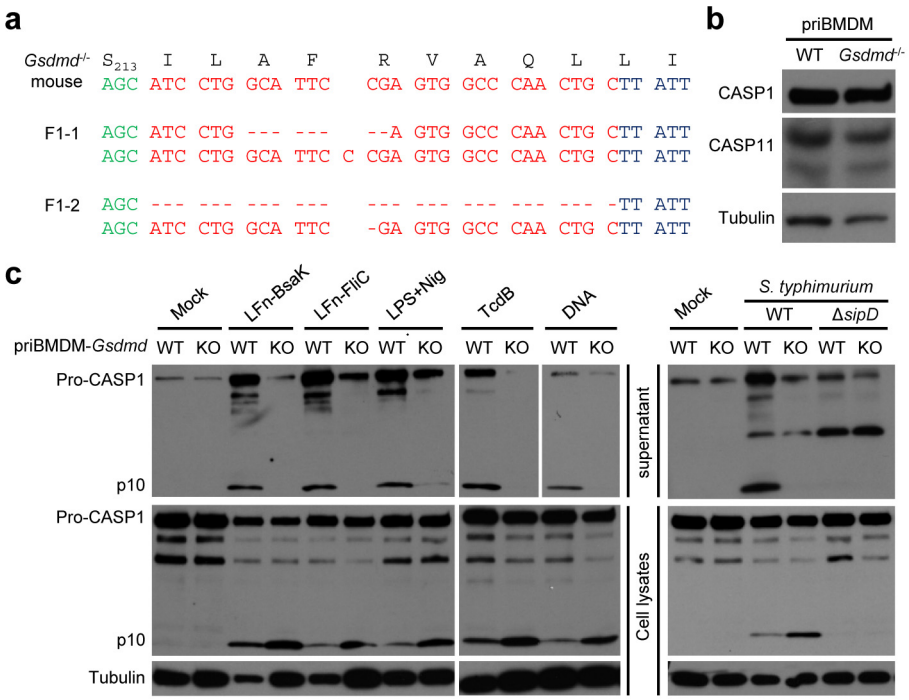

Extended Data Figure 6 | Generation of *Gsdmd*$^{-/-}$ mice and assays for inflammasome-mediated caspase-1 autoprocessing and secretion. **a**, *Gsdmd*$^{-/-}$ mice were generated by CRISPR-Cas9-mdiated targeting. Shown are the sequence mutations in the two homozygous F1 lines (F1-1 and F1-2) used in the study. **b**, Anti-caspase-1/caspase-11 immunoblots of lysates of unstimulated primary BMDM cells derived from wild-type and *Gsdmd*$^{-/-}$ mice. **c**, Primary BMDMs derived from wild-type or *Gsdmd*$^{-/-}$ mice were stimulated with indicated canonical inflammasome stimuli or infected with *S. typhimurium* (wild type or the T3SS-deficient Δ*sipD* mutant). Total cell lysates or the culture supernatants were subjected to anti-caspase-1 or anti-tubulin immunoblotting. Data shown (**b**, **c**) are representative of two independent experiments.

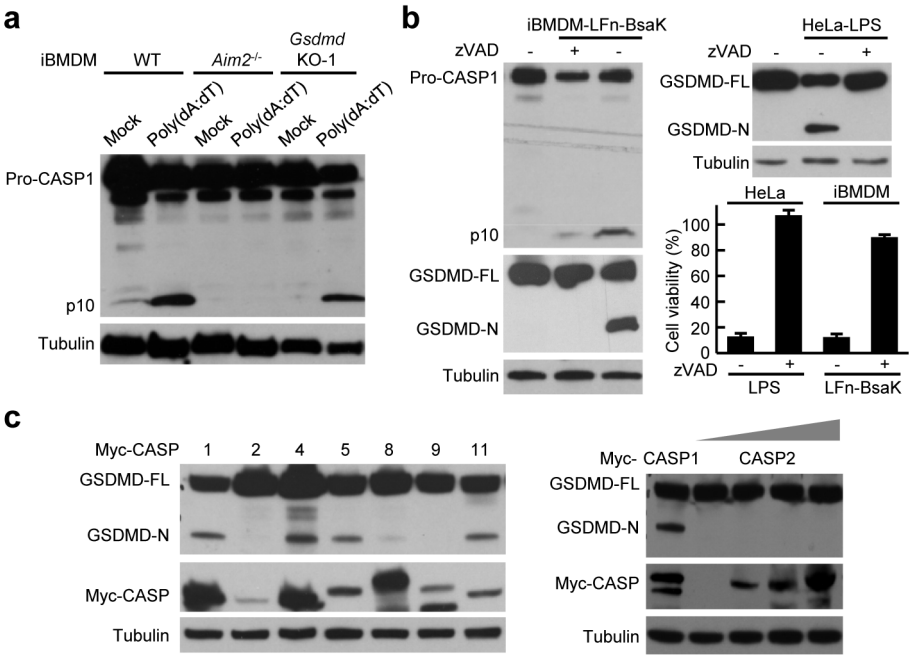

Extended Data Figure 7 | Specific cleavage of GSDMD by inflammatory caspases. **a**, Effects of *Gsdmd* knockout on caspase-1 activation by the AIM2 inflammasome. Indicated iBMDM cells were stimulated by poly(dA:dT) transfection. **b**, Effects of the pan-caspase inhibitor zVAD on LPS electroporation- and LFn–BsaK-induced GSDMD cleavage in HeLa and iBMDM cells, respectively. ATP-based cell viability is expressed as mean values ± s.d. from three technical replicates. **c**, Assays of GSDMD cleavage by inflammatory and apoptotic caspases overexpressed in cells. 3×Flag–GSDMD was co-transfected with indicated Myc–caspase into 293T cells. Total cell lysates were analysed by anti-caspase-1 (**a**, **b**), anti-Flag (**b**, **c**), anti-Myc (**c**) and anti-tubulin (**a**–**c**) immunoblotting. Data shown are representative of three independent experiments.

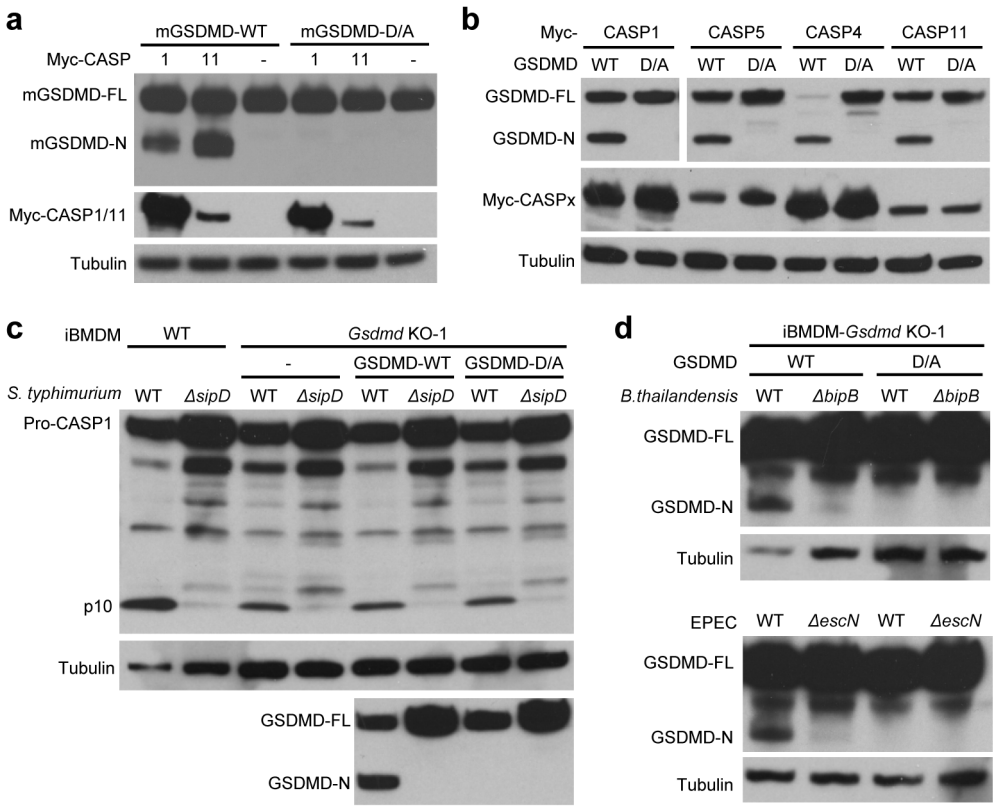

Extended Data Figure 8 | Resistance of the GSDMD D/A mutant to inflammatory-caspase cleavage. **a**, **b**, Assays of proteolytic cleavage of the GSDMD D/A mutant by overexpression-activated inflammatory caspases. 3×Flag-tagged mouse (**a**) or human (**b**) GSDMD (wild-type or the D/A mutant) was co-transfected with Myc-tagged caspase-1/11 (**a**) or caspase1/4/5/11 (**b**) into 293T cells. Cell lysates were analysed by anti-Flag, anti-Myc and anti-tubulin immunoblotting. **c**, **d**, Assays of proteolytic cleavage of GSDMD D/A mutant by bacterial-infection-activated caspase-1. Wild-type, *Gsdmd* knockout (the KO-1 clone), or *Gsdmd* KO-1 complemented with 2×Flag–HA–GSDMD (wild-type or the D/A mutant) iBMDM cells were infected with wild-type *S. typhimurium* (**c**), *B. thailandensis* or EPEC (**d**) to induce caspase-1 activation (by the NAIP–NLRC4 inflammasome), or their T3SS-deficient mutant strains (Δ*sipD*, Δ*bipB* and Δ*escN*, respectively) as controls. Cell lysates were analysed by anti-caspase-1, anti-tubulin and anti-Flag immunoblotting. p10, mature caspase-1. GSDMD-FL, full-length GSDMD; GSDMD-N, the N-terminal cleavage product of GSDMD. The D/A mutants refer to D275A for human GSDMD and D276A for mouse GSDMD. Data shown are representative of three independent experiments.

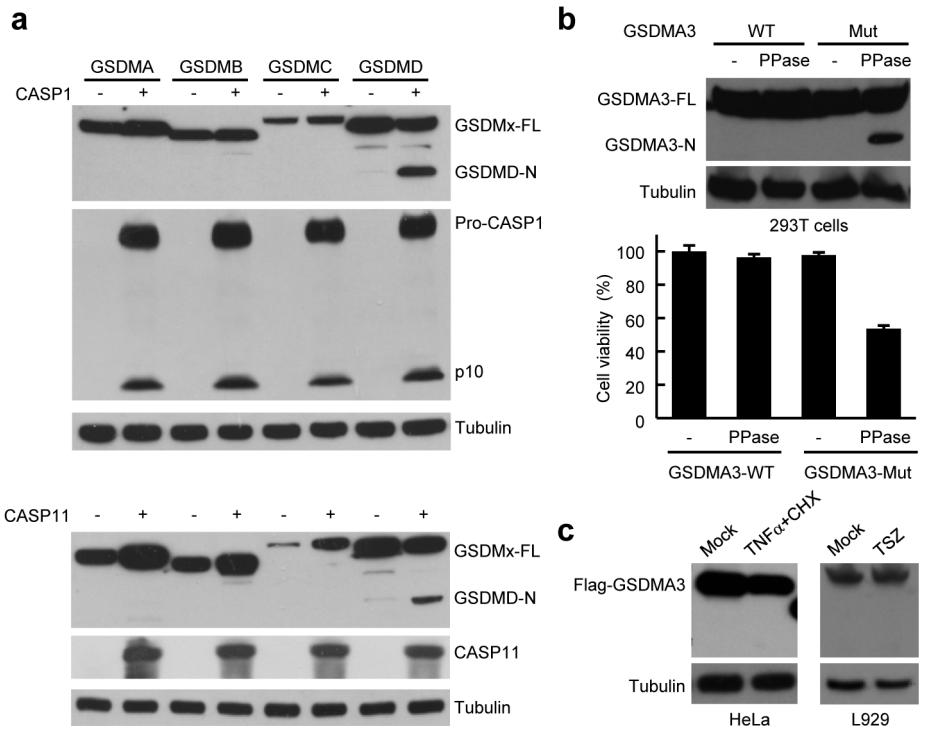

Extended Data Figure 9 | Characterization of GSDMA3 and other gasdermin family members. **a**, Flag-tagged GSDMA, GSDMB, GSDMC and GSDMD were co-transfected with caspase-1 (upper panel) or caspase-11 (lower panel) into 293T cells. Cell lysates were analysed by anti-Flag, anti-caspase-1, anti-Myc or anti-tubulin immunoblotting. **b**, Wild-type GSDMA3 or a GSDMA3-mutant harbouring a PPase cleavage site between its gasdermin-N and -C domain was expressed in 293T cells. Recombinant PPase was transfected into the cells by electroporation. The upper panel shows the immunoblots of cell lysates to examine GSDMA3 cleavage and the lower panel shows ATP-based cell viability expressed as mean values ± s.d. from three technical replicates. **c**, The absence of GSDMA3 cleavage in TNFα-induced apoptosis and necroptosis. Flag–GSDMA3 was expressed in HeLa and L929 cells. Apoptosis was induced by TNFα + CHX treatment in HeLa cells and necroptosis was induced by TSZ stimulation of L929 cells. Lysates of stimulated cells were analysed by anti-Flag and anti-tubulin immunoblotting. Data shown are representative of three independent experiments.